Estimating the Yield of Rice Farms in Southern Iraq using Landsat images

S.M. Ali[1] S.S. Salman[2]
[1&2]University of Baghdad, Iraq, Baghdad, Al- Jaderyia
[1]College of Science, Remote Sensing Research Unit [2]College of Pharmacy
[1]smalitokmachi@scbaghdad.edu.iq [2]salma3_sultan@yahoo.com

Abstract: Forecasting rice yield before harvest time is important to supporting planners and decision makers to predict the amount of rice that should be imported or exported and to enable governments to put in place strategic contingency plans for the redistribution of food during times of famine. This study used three Vegetation Indices (i.e. NDVI, EVI, and RGVI) to predict the amount of rice yields from temporal satellite imagery (i.e. Landsat 7 and 8) for the periods 2012 and 2014. Scatterplot classification technique is also implemented to estimate the rice yield for the same periods. The estimated results obtained by both the vegetation indices and the scatterplot classification techniques have been compared with true amount of the rice product for the same periods to verify the validity of the adopted methods.

Index Terms— Vegetation Indices, NDVI, EVI, RGVI, Rice Yield Estimation, Scatterplot Classification

1 INTRODUCTION

Rice is one of the most important agriculture crops in many countries. It is a primary food source for more than three billions of people worldwide [1]. Forecasting rice yield before harvest is crucial, especially in regions characterized by climatic uncertainties. It enables planners and decision makers to deduce how much to import in the case of a shortfall or, optionally, to export in the case of a surplus. Forecasting also allows governments to develop a strategic contingency plans for distribution the food during times of famine. Therefore, monitoring the growth and development of plants with guesses of the production yield possess a great importance [2]. Over the past twenty-five years, the multispectral images taken by satellites have proven as to be a powerful tool in determining the amounts of the productivity of agricultural crops [3-4]. An important goal of agricultural remote sensing research is to spectrally estimate crop variables related to crop conditions, which can subsequently be entered into crop simulation and yield models [5].

To utilize the full potential of remote sensing for the assessment of crop conditions and yield prediction, it is essential to quantify the relationships between the agronomic parameters and spectral properties of the crop [6]. Use of satellite spectral data for the estimation of crop yields is an attractive prospect because yield is related to crop vigor (i.e. related to the spectral response of the crop activity), which in turn is related to the spectral response of the crop measured by satellite sensors [7].

In fact, the correlation between the spectral reflectance of crops and their agronomic variables has encouraged many researchers to use it for developing crop yield models [8]. Some of the researches utilized the global resolution satellite images (e.g. MODIS, SPOT, MSS, TM, ETM_+, etc.) to estimate the expected rice yield. Too many studies have used the satellite imaging to monitor rice growth, for instance see [9-10]. Some of these researches have used low and moderate image resolution; e.g. National Oceanic and Atmospheric Administration (NOAA), Advanced Very High Resolution Radiometer (AVHRR) and Moderate Resolution Imaging Spector radiometer (MODIS), to monitor rice fields, for instance see [9 and 11].

However, the use of low and moderate spatial resolution of satellite imaging has been restricted, particularly in small rice areas because many types of land cover appear in few pixels, which reduces the accuracy of the assessment.

The Landsat program is the longest running enterprise for acquisition of satellite imagery. It is started on July 23, 1972 when the first was launched, it was known as the Earth Resources Technology Satellite (ERTS), carried two of instruments: a camera system (called Return Beam Vidicon "RBV"), and Multispectral Scanner (MSS) recorded data in four spectral bands (i.e. green, red, and two infrared bands). The most recent, Landsat 8, was launched on February 11, 2013, it consists of eleven spectral bands, eight of them with a spatial resolution of 30 meters (i.e. bands 1 to 7 and 9), The resolution for Band 8 (panchromatic) is 15 meters. Two thermal infrared bands (i.e. 10 and 11) of spatial resolution 100 meters each scene cover an area of 170×183 km^2. It is also worthwhile to mention the specifications of Landsat-7 images that have been used in the current study. Images consist of eight spectral bands with a spatial resolution of 30 meters for bands 1 to 5 and 7, while band 6 (thermal of 60 meters), and band 8 (panchromatic) is 15 meters. Again, each scene covers an area of size 170×183 km^2. The objective of the current study is to provide an overview of the use of remote sensing imagery for mapping rice crop areas and forecasting its production. Furthermore, reviewing the suitability of remote sensing-based methods for mapping rice areas and their limitations, and testing their potentiality in forecasting rice yield and their functional implication

2 The Study Area

The study area ***Al-Najaf and Al-Qadisiya*** district, shown in Figure1, is a fertile mudslides land area, about 30 km south of **Najaf province**, 230 km southwest of the **Baghdad** (capital of Iraq). A river (called **Al-Hidia**) of length 25km, which is part of the **Euphrates River**, passes through the study area. The study area is surrounded by rice plantations and palm groves.

Administrative map of Iraq showing the international and local borders between the provinces. The country lies between the geographic coordinates lat.37.38°→ 28.5°N, and Long. 38.70°→48.75°E.

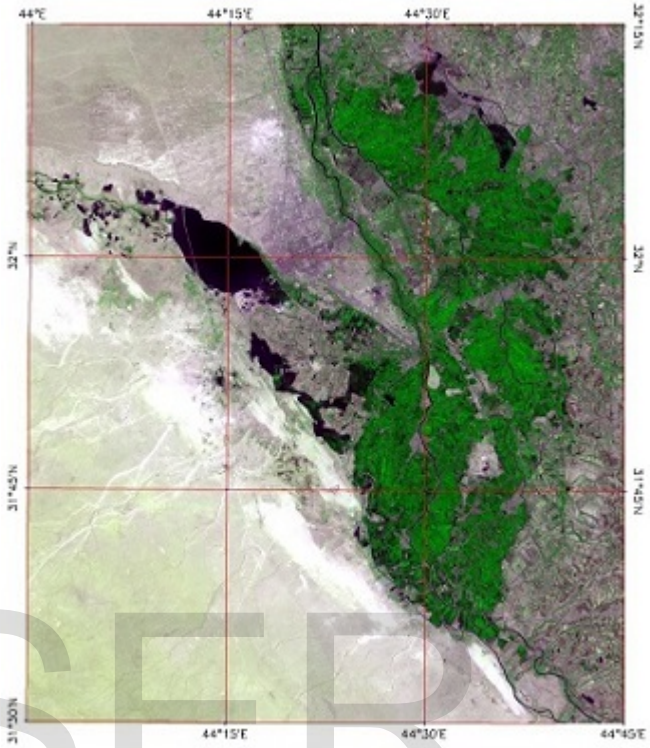

Photomap of the study area ***Al-Najaf and Al-Qadisiya*** district, Located in the south of the ***Najaf*** province in the middle-south of Iraq, Lat.32.216°→31.550° N, and Long. 44.161°→ 44.724°E. It is an agricultural area specialized in planting rice

Figure1 Administrative map of Iraq country and photomap of the study area

3 Preparing Landsat Images

As mentioned above, the study based on using the vegetation indices and the scatterplot classification techniques on Landsat multispectral images to estimate the amount of the rice productivity cultivated in the study area (***Al-Najaf and Al-Qadisiya***). The main source we have adopted to get multispectral band images for the study area was from the ***USGS Global Visualization Viewer of the Earth Resources and Science Center (EROS)*** [http://glovis.usgs.gov/]. The study area is path/Row (168/38). When we dealt with **Landsat-7** (i.e. **ETM+**) images, we have encountered by another problem: i.e. the presence of gapes due to the failure of ***Scan Line Corrector*** (***SLC***) occurred on May 31, 2003. Consequently, all ETM+ images after May 31, 2003 have been greatly affected by the failure and have lost approximately 22% of their data, appear as gaps [12], as illustrated in Figure 2.

A number of digital techniques have been developed and introduced to bridge the gaps in the Landsat-7 (ETM+), [12]. The majority of the introduced methods used two scenes (taken at different times) to bridge the gaps by transferring pixel values from the undistorted areas of the assisted image to corresponding gap locations in the processed (reference) image. Since the corrected images are required to predict the amount of crop yield, which are subject to change in short periods of time, as well as to the difficulty in obtaining ETM+ scenes taken in a short interval of time, so in our current research we have adopted gaps bridging methods based on the neighborhood to estimate the gap's values. Two methods have been adopted; i.e.

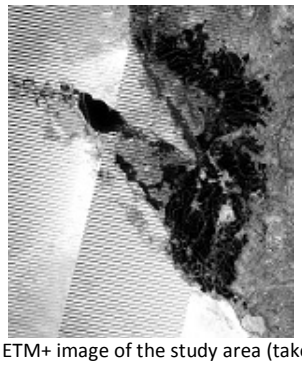

Figure 2 Extracted ETM+ image of the study area (taken in 07-09-2014), with gaps

1. In the first method, the gaps locations were filled by the median value, utilizing large neighborhood window (size 11×11 pixels), the result is illustrated in Figure 3.
2. In the second method, the ENVI software was utilized to replace the gaps locations (considering them as bad values). The gap's bridging process uses Delaunay triangulation to fill the bad pixels with triangles calculated from the surrounding good values (Lee et al., 1980). The result is illustrated in Figure 4.

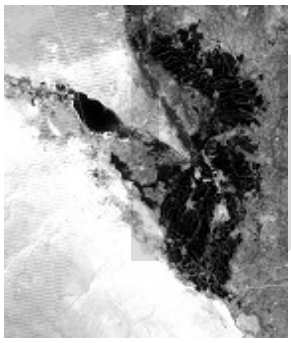

Figure 3 Restored image of study area by median filter of window's size 11×11 pixels

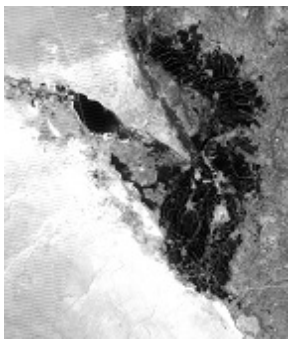

Figure 4 Restored image of study area by replacing the bad (zero) values

4 Converting Landsat DNs to Top of Atmosphere (ToA) Reflectance

The Landsat sensors capture reflected solar energy, convert them to radiance, and then rescale those data into an 8bits digital number "DN" (range from 0 →255) for the Landsat-7 ETM+ sensor, and into 16bits (range from 0 → 65536) for the Landsat-8 OLI sensor. The OLI band data can also be converted to TOA planetary reflectance using reflectance rescaling coefficients provided in the product metadata file (MTL file) that is provided by (http://landsat.usgs.gov/Landsat8 Using Product.php). The following equation is used to calibrate DN values to TOA reflectance for OLI data as follows:

$$\rho_\lambda = \frac{M_\rho Q_{cal} + A_\rho}{\cos(\theta_{Sz})} \quad (1)$$

Where: ρ_λ = TOA planetary reflectance, M_ρ = Bandspecific multiplicative, A_ρ = Bandspecific additive, Q_{cal} = Quantized and calibrated standard product pixel values (DN), ϑ_{SZ} = Local solar zenith angle; ϑ_{SZ} = 90° - ϑ_{SE} where ϑ_{SE} = Local sun elevation angle. Figure 5 represents the absolute difference between the LandSat-8 (September 2014) image and its TOA calibrated version.

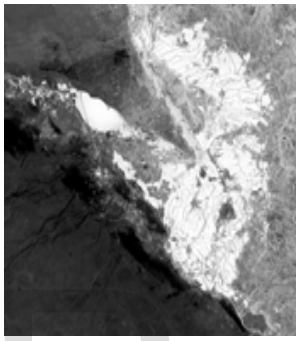

Figure 5 Absolute differences between original Landsat-8 and its TOA calibrated images of (September 2014)

The Landsat-7 band data can also converts to TOA, using the following calibration equation [13]:

$$\rho_\lambda = \frac{\pi L_\lambda d^2}{ESUN_\lambda \cos(\theta_{Sz})} \quad (2)$$

Where: L_λ= Spectral radiance at the sensor's aperture, d= Earth–Sun distance, $ESUN_\lambda$= Mean exoatmospheric solar irradiance, and ϑ_{SZ} as defined in Eq. (1).

Figure 6 represents the absolute difference between the LandSat-7 (September 2014) image and its TOA calibrated version.

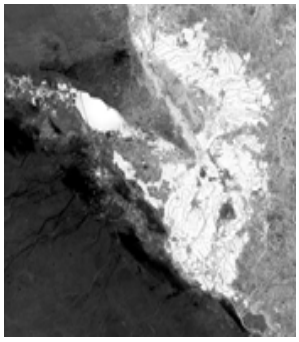

Figure 6 Absolute differences between original Lansat-7 and its TOA calibrated image of (September 2014)

5 Research Prediction Methods

As mentioned in beginning of this paper, the mapping distribution processes of rice plants will utilize two types of Landsat images (i.e. 7 and 8), using two approaches (i.e. vegetation indices and scatterplot classification method), as will be given below:

5.1 Vegetation Indices

The remote sensing based methods have been widely used for mapping rice areas worldwide, for instance see [9-10]. The satellite sensors have the potential of obtaining multi-temporal and multi-spectral reflectance data over croplands that can be used for deriving time-series of vegetation indices (VIs), calculated as a function of the provided images by currently operating satellites. The pigment in plant leaves (i.e. ***chlorophyll***) and its behave in strongly or weakly absorbing or reflecting certain electromagnetic sun rays falling on them which is important for conducting the ***photosynthesis*** process. Among the too many indices that have been developed and introduced for monitoring the crop growth, we have selected the most common used of them to be implemented in this research, mentioned in TABLE 1, [11].

TABLE 1
List of the common vegetation indices, and their mathematical formula, used to monitoring the crop growth and yield forecasting

Index	Formula
Normalized Difference Vegetation Index NDVI	$\frac{\rho_{NIR}-\rho_{Red}}{\rho_{NIR}+\rho_{Red}}$
Enhanced Vegetation Index EVI	$\frac{\rho_{NIR}-\rho_{Red}}{\rho_{NIR}+6\times\rho_{Red}-7.5\times\rho_{Blue}+1}$
Rice Growth Vegetation Index RGVI	$1-\frac{\rho_{Blue}+\rho_{Red}}{\rho_{NIR}+\rho_{SWIR1}+\rho_{SWIR2}}$

Note: ρ is the surface reflectance values for near infrared (NIR), and shortwave infrared (SWIR1and SWIR2)

4.2 Comparing NDVI of Landsat- 8 and Landsat-7 imageries

Dates of the images used in this research have been adopted to represent the peak of vegetative growth in the studied rice fields (i.e. September 2012 and 2014). Unfortunately, there is a time difference (8 days) in the passage of the Landsat satellites (7 and 8) over the same area. This difference in time means a clear change in the vegetative growth of crops, causing slight changes in the NDVI measurements. Therefore, the NDVI scatterplots between the Landsat images acquired at (7 Sep. and 23 Sep. 2o14) with images of Landsat-8 acquired at (18 Sep. 2014) show large differences, as illustrated in Figure 7.

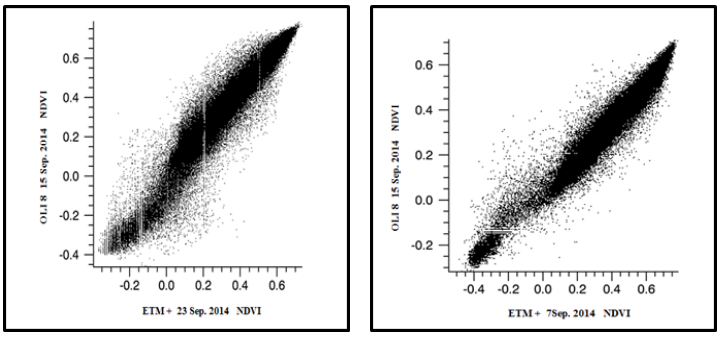

Figure 7 Comparison between NDVI-scatterplots of Landsat-8 and Landsat-7 acquired in different times

To avoid the effects of phenology within the 8 day interval between Landsat 7 and 8 images, ***vegetation growth rate*** relationship was developed by [14] for cropland, grassland and shrub land to correlate with Landsat-8 NDVI of 15 Sep. 2014 with Landsat-7 NDVI of 7 and 23 Sep. 2014. The vegetation growth rate for Landsat-7 NDVI (for the periods 7&23Sept. 2014) compared with the Landsat-8 NDVI (of 15Sep. 2014) is given by:

$$r=\frac{(NDVI)_{23Sep}-(NDVI)_{15Sep}}{(NDVI)_{15Sep}-(NDVI)_{7Sep}} \quad (3)$$

The simulate Landsat-7 NDVI of 15 Sept. 2014 then given by;

$$NDVI_{15Sep.}=\frac{(NDVI)_{23Sep}+r\times(NDVI)_{7Sep}}{1+r} \quad (4)$$

Figure 8 shows the scatterplot drawn between the simulated Landsat-7 NDVI (i.e. $NDVI_{15Sep.}$) and the Landsat-8 NDVI acquired at 15Sept. 2014.

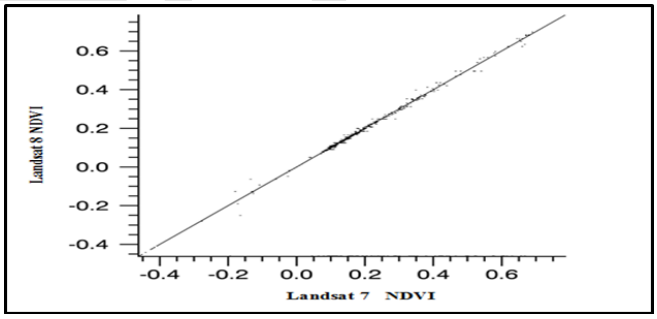

Figure 8.Scatterplot between simulated Landsat-7 NDVI with Landsat-8 NDVI

As it is obvious, the linear relationship between the NDVI of Landsat-8 and the simulated NDVI of Landsat-7 indicates a high degree of correlation has been achieved using the vegetation growth rate presented by Equations (3 & 4)

5.3 Scatterplot Classification Method

It is well known that the soil has property which shows a linear relationship between "*NIR*" and "*Red*" reflectance bands. The length of the linearity between the "*NIR*" and "*Red*" responses is affected by the soil's dryness or wetness contents; i.e. it is shortened for homogenous soils, and extended as the soil's

contents varies. Therefore, as the soil line is defined, the corresponding reflectance regions of the other spectral classes can be decided accordingly. These behaviors have been benefited by Ali (2013) to introduce an automatic multispectral image classification based on scatterplot method. This classification method will be utilized to predict the vegetated area in the images of the study area.

6 Results and Discussions

The results in this section will be divided into two parts; in the first part the three adopted vegetation indices (i.e. NDVI, EVI, and RGVI) will be used to estimate the dense vegetated areas and, consequently, the productive rate of the rice yield in the study area. In the second part, the scatterplot classification method will be implemented to predict the productivity of the rice yield.

6.1 Vegetation Indices

As indicated before, three vegetation indices will be adopted to perform the rice yield prediction; i.e.

6.1.1 Normalized Difference Vegetation Index (NDVI)

It is one of the most widely used vegetation index which is typically derived from observations from the Advanced Very High Resolution Radiometer (AVHRR). The ***NDVI*** values range between [-1, +1]. According to the ***United States Geological Survey*** (***USGS***) remote sensing phenology studies used to measure wavelengths of light absorbed and reflected by green plants. The ***NDVI*** values are categorized as follows; areas of barren rock, sand, or snow usually show very low NDVI values (e.g. ***0.1 or less***). Sparse vegetation such as shrubs and grasslands or senescing crops may result in moderate ***NDVI*** values (i.e. approximately ***0.2 to 0.5***). High ***NDVI*** values (approximately ***0.4 to 0.8***) correspond to dense vegetation such as that found in temperate and tropical forests or crops at their peak growth stage. In our current study area, the cultivation of rice begins in mid of June. Accordingly, the maximum greenness stage is expected in mid of September (i.e. three months later). Therefore, it is expected to increase the assessment rates of vegetative area whenever was closer to September. Figure 9 shows the NDVI images acquired by; (1) Landsat-8 OLI sensor at September 2014, and (2) Landsat-7 ETM+ sensor at September 2014.

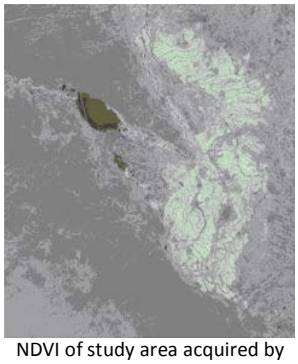

NDVI of study area acquired by LandSat-8 at September 2014

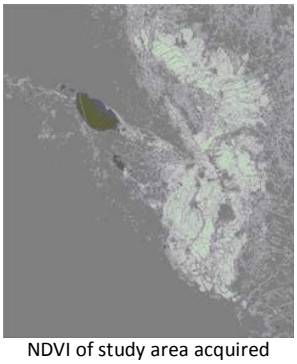

NDVI of study area acquired by LandSat-7 at September 2014

Figure 9 NDVI images for the study area using Landsat 8&7 bands

The dense vegetative areas of Figure 9 have been isolated (i.e. **0.4 ≤ NDVI ≤ 0.8**), and their areas were calculated and illustrated in Figure10. Note: Area = No. of pixels×30×30 m^2/10000 Hectares

Dense vegetation area 83170 Hectares, Landsat-8, at September 2014

Dense vegetation area 83170Hectares, Landsat-7,at September 2014

Figure 10 Extracted dense vegetation areas, using NDVI

6.1.2 Enhanced Vegetation Index (EVI)

In December 1999, NASA launched the Terra spacecraft, the flagship in the agency's Earth Observing System (EOS) program. Aboard Terra flies a sensor called the ***Moderate-resolution Imaging Spectroradiometer***, or ***MODIS***, that greatly improves scientists' ability to measure plant growth on a global scale [15]. The MODIS science team prepared a new data product–called the ***Enhanced Vegetation Index*** (***EVI***) to improve the quality of the ***NDVI*** product. While the ***EVI*** is calculated similarly to ***NDVI***, it corrects for some distortions in the reflected light caused by the particles in the air as well as the ground cover below the vegetation. The ***EVI*** was developed to optimize the vegetation signal with improved sensitivity in high biomass regions and improved vegetation monitoring through a de-coupling of the canopy background signal and a reduction in atmosphere influences. The equation was of the form,

$$EVI = G\frac{\rho_{NIR} - \rho_{\mathrm{Red}}}{\rho_{NIR} + C_1 \times \rho_{red} - C_2 \times \rho_{Blue} + L} \qquad (5)$$

Where: *G* is gain factor, *L* is the canopy background adjustment that addresses nonlinear, differential ***NIR*** and ***Red*** radiant transfer through a canopy, and C_1, C_2 are the coefficients of the aerosol resistance term, which uses the blue band to correct for aerosol influences in the red band.

The coefficients adopted in the ***EVI*** algorithm are, *L=1*, C_1=6, C_2 = 7.5, and G = 1.0, [16]. The final equation form is as it given in table 1. The *EVI* values range [-1, 1]. Figure 11 shows the dense vegetation area's images acquired by the same sensors of Figure 9.

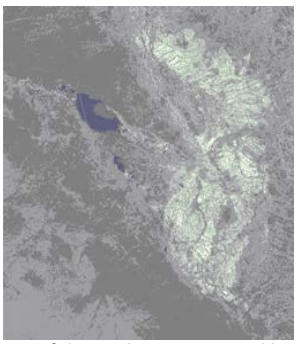
EVI of the study area acquired by LandSat-8 at September 2014

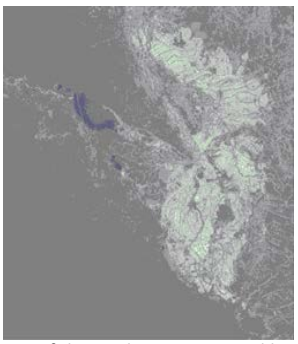
EVI of the study area acquired by LandSat-7 at September 2014

Figure 11 EVI images for the study area using Landsat 8&7 bands

The dense vegetative areas of Figure 11 have been isolated (i.e. ***0.4 ≤ EVI ≤ 0.8***) and illustrated in Figure 12.

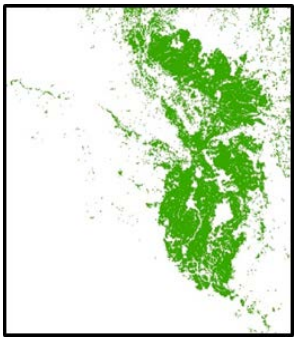
Dense vegetation area 65747.5Hectares, Landsat-8, at September 2014

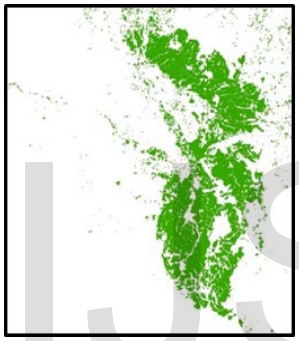
Dense vegetation area 58697.5Hectares, Landsat-7, at September 2014

Figure 12 Extracted dense vegetation areas, using EVI

6.1.3 Rice Growth Vegetation Index (RGVI)

Rice like other vegetation contains chlorophyll pigments in its leaves that absorb red light and radiate NIR portion. This interaction between leaves and the light is often determined by their different responses in the red and NIR portions of the reflective light. In contrast, absorption properties of the middle infrared band cause a low reflectance of rice plants [17]. In irrigated rice fields, especially in early transplanting periods, water environment plays an important role in rice spectral. The ρ_{Blue} band of Landsat has good sensitivity to the existence of water; consequently it is desirable for the rice growth vegetation index (RGVI) to use the following Landsat bands; blur, red, near-infrared, and the shortwave infrared bands SWIR1and SWIR2, using the RGVI equation listed in Table 1. The RGVI values range [-0.02, 1.44]. Figure 13 shows the RGVI dense vegetation area's images acquired by the same sensors of Figure 9.

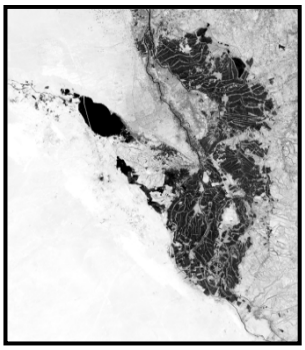
RGVI of study area acquired by LandSat-8 at September 2014

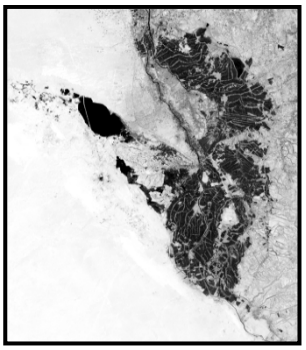
RGVI of study area acquired by LandSat-7 at September 2014

Figure 13 RGVI images for the study area using Landsat 8&7 bands

The dense vegetative areas of Figure 13 have been isolated (i.e.0.8 ***≤ RGVI ≤ 0.94***) and illustrated in Figure 14.

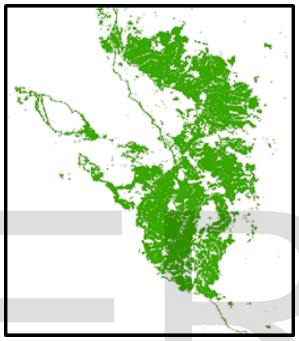
Dense vegetation area 66547.5Hectares, Landsat-8,at September 2014

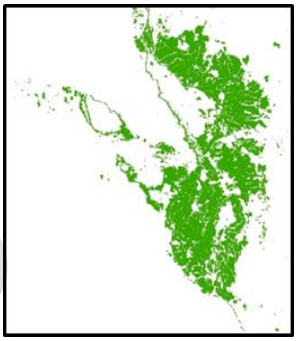
Dense vegetation area 66860Hectares, Landsat-7,at September 2014

Figure 14 Extracted dense vegetation areas, using RGVI

6.2 Scatterplot Classification

As was mentioned before, the rice yield prediction in this study utilizes two methods. The vegetation indices (as was conducted above) and the classification method based on the scattering behaviors of the Landcover components. One efficient way to implement this classification method is that provided by [18]. The method is based on dividing the scatterplot diagram of the Red and NIR bands into regions corresponding to the reflectance values of the Landcover components (i.e. dry soil, wet soil, dry vegetation, wet vegetation, dense-healthy vegetation, and water areas), as illustrated in Figure 15.

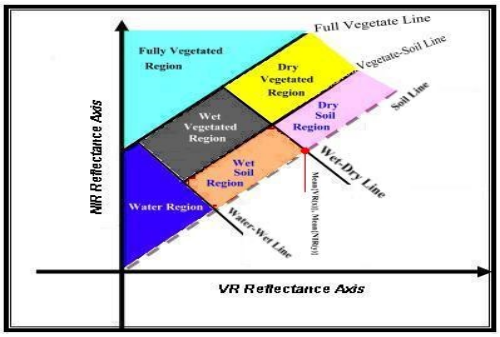

Figure 15 Classification Scheme Based on Scatterplot

Figure 16 shows the scatterplot classification result of the study area, performed on both Landsat 7&8 images.

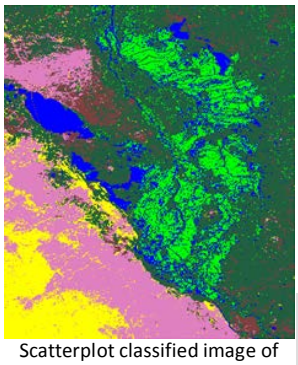

Scatterplot classified image of study area acquired by LandSat-8 at September 2014

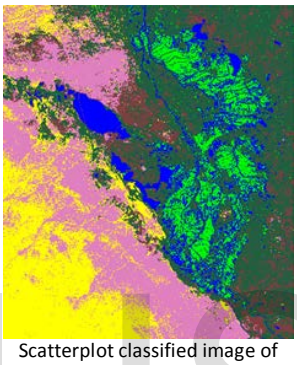

Scatterplot classified image of study area acquired by LandSat-7 at September 2014

Figure 16 Scatterplot classification of study area, using Landsat 8&7 bands

The dense vegetation areas obtained by implementing the scatterplot classification method are illustrated in Figure 17.

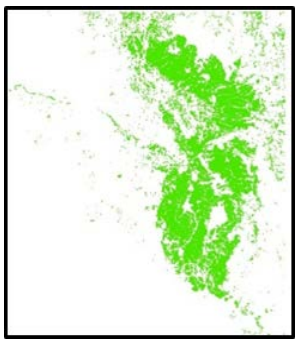

Dense vegetation area 575925 Hectares, Landsat-8, at September 2014

Dense vegetation area 44025Hectares, Landsat-8, at September 2014

Figure 17 Extracted dense vegetation areas obtained by implementing the scatterplot classification method

Table 2 shows the accuracy of the calculated acreage by using the vegetation indices and the scatterplot classification techniques compared with the actual acreage for the years 2012 and 2014 that have been obtained from the ***publications of the Iraqi Ministry of Agriculture***; i.e. 67500 Hectares in 2012, and 72807 Hectares in 2014.

TABLE 2
Estimation area and its accuracy

Data used	Predictive (Agriculture area) Hectares	Accuracy
NDVI		
Landsat 8 (2014)	83170	86%
Landsat 7 (2014)	83170	99%
Landsat 7 (2012)	68005	99%
EVI		
Landsat 8 (2014)	65747.5	90%
Landsat 7 (2014)	58697.5	80%
Landsat 7 (2012)	52037.5	77%
RGVI		
Landsat 8 (2014)	66547.5	91%
Landsat 7 (2014)	66860	91.8%
Landsat 7 (2012)	51284	76%
Scatterplot Classification		
Landsat 8 (15/9/2014)	575925	80%
Landsat 7 (23/9/2014)	44025	60%
Landsat 7 (17/9/2012)	36247.5	54%

7 CONCLUSIONS

In this paper, the cultivated areas of the rice farms in the provinces of Najaf and Al-Qadisiya south of the Iraqi country have been calculated, using the vegetation indices and scatterplot classification techniques. Through the research course we have faced many problems, these were: The presence of gaps in the Landsat-7 (ETM+) images due to the failure of its ***scan line corrector***. This problem was overcome by bridging those gaps by first utilizing the ***median filter*** of large window's size, and second by the gaps (zero values) as to be undesirable (bad values) and replacing them by utilizing the Delaunay triangulation restoration method. In both these restoration methods, substituted values may not represent the true vegetative cover due to the rapid growth rates of the crops and the juxtaposition of the vegetated area with other varieties of ground cover components. In fact, replacing the gap's values by same position pixel values in another time asymptotic scene would cause the same error also because the fast vegetative growth rates. Therefore, it is expected that the research results does not match with the true published values of the cultivated areas.

The second problem we have faced was that the scenes acquired by different satellites have different timings in passing over the study area. Again because of the rapid rates of vegetative growth, acreage estimated areas may vary from one scene to another. To overcome this problem we have calibrated the NDVI images, using the vegetation growth rate relationship (Eq.(3&4)). The simulated NDVI

showed high correlation with that produced by another satellite image and acquired in different time (Figure 8).

The Last problem we have encountered was the lack of accurate records issued by the Iraqi Ministry of Agriculture for the true acreage. For this purpose, research team has visited the study area carrying GPS device to install the farm's sites and make sure the information was correct.

Finally, we believe that the use of high-resolution images (e.g. of the French satellite "SPOT", resolution 2.5 or 5 meter) would improve the assessment of cultivated areas.

REFERENCES

[1] C.M. Yang, C.C. Liu, and Y.W. Wang, "Using Formosat-2 Satellite Data to Estimate Leaf Area Index of Rice Crop," Journal of Photogrammetry and Remote Sensing, 13, 253–260, 2008.

[2] H.L.S. Sawasawa, "Crop Yield Estimation: Integrating RS, GIS, and Management Factor: A case study of Birkoor and Kortigiri Mandals, Nizamabad District India," MSc Thesis, 2003. Available on http://www .itc .nl /library /papers_2003 / msc/nrm/sawasawa.pdf.

[3] A. Bouvet, T. Toan, and N. Lam-Dao, "Monitoring of the Rice Cropping System in the Mekong Delta Using ENVISAT/ASAR Dual Polarization Data," IEEE Trans. Geoscience and Remote Sensing, 47, 517 – 526, 2009

[4] I.W. Nuarsa, and F. Nishio, "Relationships between Rice Growth Parameters and Remote Sensing Data," International Journal of Remote Sensing and Earth Sciences, 4, 102-112, 2007.

[5] J.S. Ahlrichs, and M.E. Bauer, "Relation of agronomic and multispectral reflectance characteristics of spring wheat canopies," Agronomy Journal, 75, 987-993, 1983.

[6] I.W. Nuarsa, F. Nishio, and C. Hongo, "Spectral Characteristics and Mapping of Rice Plants Using Multi-Temporal Landsat Data," Journal of Agriculture Science, 3, 54-67, 2011.

[7] T.L. Barnett, and D.R. Thompson, "The use of large-area spectral data in wheat yield estimation," Remote Sensing of Environment, 12, 509-518, 1982.

[8] Y. Shao, X. Fan, H. Liu, J. Xiao, S. Ross, B. Brisco, R. Brown, and G. Staples, "Rice Monitoring and Production Estimation Using Multi-temporal RADARSAT," *Journal of Remote Sensing for Environment*, 76, 310–325, 2001.

[9] S. Panigrahy, J.S. Parihar, and N.K. Patel, "Kharif rice acreage estimation in Orissa using NOAA-AVHRR data," *Journal of the Indian Society of Remote Sensing*, 20, 35-42, 1992.

[10] D. David, S. Frolking, and C. Li, "Trends in Rice-Wheat Area in China," *Field Crops Research*, 87, 89-05, 2004.

[11] K.M. Mostafa, K.Q. Hassan, and E.H. Chowdhury, "Application of Remote Sensors in Mapping Rice Area and Forecasting Its Production," A Review, *Sensors* 2015, *15*, 769-791, 2005.

[12] T. Wataru, O. Taikan, and Y. Yoshifumi, "Investigating an integrated approach on rice paddy monitoring over Asia with MODIS and AMSR-E," *Proceedings of the Conference of the Remote Sensing Society of Japan*, 40, 173-174, 2006..

[13] S.M. Ali, and M.J. Mohammed, "Gap-Filling Restoration Methods for ETM+ Sensor Images," Iraqi Journal of Science, Vol.54, No.1, 206-214, 20013.

[14] G. Chander, B.L. Markham, D.L. Helder, "Summary of current radiometric calibration coefficients for Landsat MSS, TM, ETM+, and EO-1 ALI sensors," Remote Sensing of Environment 113, 893–903, 2009.

[15] D. Xu, and X. Guo. "Compare NDVI Extracted from Landsat 8 Imagery with that from Landsat 7 Imagery," *American Journal of Remote Sensing,* Vol. 2, No. 2, 10-14, 2014.

[16] D.T. Lee, and B. J. Schachter, "Two Algorithms for Constructing a Delaunay Triangulation," *International Journal of Computer and Information Sciences, Vol. 9, No. 3,* 219-242, 1980.

[17] A. Huete, C. Justice, and H. Liu, "Development of vegetation and soil indices for MODIS-EOS," Remote Sensing of Environment., 49, 224– 234, 1994

[18] S.M. Ali, "New Fully Automatic Multispectral Image Classification based on Scatterplot Method," International Journal of Emerging Technology and Advanced Engineering, Volume 3, Issue 10, 388-394, 2013.